Tunnelling and Underground Space Technology 140 (2023) 105292

Contents lists available at ScienceDirect

Tunnelling and Underground Space Technology incorporating Trenchless Technology Research

journal homepage: www.elsevier.com/locate/tust

Performance of road tunnel subjected to BLEVE occurring inside adjacent tunnel

Ruishan Cheng [a], Wensu Chen [a,*], Hong Hao [b,a,*], Jingde Li [a]

[a] Center for Infrastructural Monitoring and Protection, School of Civil and Mechanical Engineering, Curtin University, Australia
[b] Earthquake Engineering Research & Test Center, Guangzhou University, China

ARTICLE INFO

Keywords:
Tunnel response
BLEVE
Rock type
Cover depth
Separation distance

ABSTRACT

Twin tunnel is a common and popular type of road tunnel. The safety of twin tunnel (i.e. with left and right branches) subjected to Boiling Liquid Expansion Vapour Explosions (BLEVEs) is important but less investigated in open literature. The present study numerically investigates the dynamic response of right branch of a twin-arched-tunnel subjected to a BLEVE with a 20 m^3 Liquified Petroleum Gas tanker occurring inside the left branch by using LS-DYNA. The BLEVE loads and the model of tunnel lining and rock mass subjected to blast loading have been calibrated by the authors in earlier studies. Based on the calibrated numerical model, the response of right branch of the twin-tunnel due to stress waves caused by the BLEVE occurring inside the left branch is first compared with that of the equivalent TNT explosion. It is found that the lining damage of the right branch under BLEVE-induced stress waves can be underestimated by using the TNT equivalence method. In addition, the influences of tunnel cover depths, twin-tunnel separation distances, rock types around tunnels, and concrete strengths of tunnel lining on the dynamic response of the right branch of twin-tunnel against BLEVE-induced stress waves are investigated. Compared to enhancing the concrete strength, increasing the twin-tunnel separation distance is more effective to reduce the damage of the tunnel surrounded by the rock mass with weak mechanical properties under BLEVE-induced stress waves. In addition, empirical formulae for prediction of the PPV and tensile stress on adjacent tunnel surface induced by BLEVE are proposed, which can be used for the determination of the safe separation distance between the twin tunnels against accidental BLEVE loads.

1. Introduction

Twin tunnels (closely-spaced neighbouring tunnels) have been often used in modern transportation systems to run through narrow terrains, reduce the consumption of underground space, and minimize the disturbance to adjacent structures (Cheng et al., 2021). However, it imposes challenges to ensure the safety of twin tunnels under dynamic loadings, e.g., explosions and earthquakes because the closely-spaced twin tunnels would react together to loadings and accidents occur in one tunnel would also affect another tunnel (Cheng et al., 2022b). Recently, concerns have been arisen on the behaviour of tunnel structures under the Boiling Liquid Expansion Vapour Explosion (BLEVE). The BLEVE is defined as a physical explosion due to the sudden release of pressurized vapour and superheated liquid in a transported liquefied gas or fuel tanker (Birk et al., 2019; Li and Hao, 2020). It is usually accompanied by a catastrophic failure of the transported tank due to accidental events, such as vehicle collisions and fire engulfment (Abbasi and Abbasi, 2007), etc. BLEVE accidents involving flammable substances often occur along with fires, such as pool fire, jet fire, and fireball (Birk, 1995; Hemmatian et al., 2015). When flammable fuel or gas tanks are exposed to a fire for a period, the strength of tank reduces due to the heat, leading to a rise in pressure inside the tank, which significantly increases the likelihood of a severe BLEVE (Pitblado, 2007; van den Berg et al., 2004). When a fire-involved BLEVE occurring inside a tunnel, the tunnel's lining may experience severe damage, posing a threat to the stability of the tunnel (Cheng et al., 2021). In addition, stress waves caused by BLEVE propagating in soil or rock mass around the tunnel may endanger adjacent tunnels (Cheng et al., 2022b). Previously, the authors have predicted BLEVE overpressures inside tunnels numerically and analytically (Li et al., 2022). Furthermore, the structural responses of tunnel under BLEVE overpressures were investigated (Cheng et al., 2022a; Cheng et al., 2022c). However, the influence of stress waves due

* Corresponding authors.
E-mail addresses: wensu.chen@curtin.edu.au (W. Chen), hong.hao@curtin.edu.au (H. Hao).

https://doi.org/10.1016/j.tust.2023.105292
Received 24 July 2022; Received in revised form 17 February 2023; Accepted 19 June 2023
Available online 24 June 2023

to the BLEVE inside one tunnel on the dynamic response of adjacent tunnel is still unclear, which needs be investigated for the safety of the adjacent tunnel.

By far, the tunnel behaviour due to high explosive (HE) explosion-induced stress waves originating from adjacent tunnels have been widely investigated (Feldgun et al., 2014; Li et al., 2013; Mitelman and Elmo, 2014; Zhou, 2011; Zhu et al., 2018). For instance, Zhou (2011) experimentally investigated the dynamic response of an underground tunnel subjected to multi-group TNT explosion-induced stress waves originating from an adjacent tunnel-like chamber. A slight shotcrete spalling from the tunnel wall in the study was observed under the stress waves caused by the repeated TNT explosions. Li et al. (2013) analytically derived a motion equation for a tunnel wall subjected to TNT explosion-induced waves originating from its adjacent tunnel based on the wave-field theory. It was identified that the dynamic response of the tunnel was significantly affected by the loading density (i.e., the explosive weight divided by tunnel volume). Feldgun et al. (2014) numerically analysed the response of the right branch of rectangular twin tunnels due to stress waves caused by TNT explosions inside its left branch via a variational-difference method. It was found that the right branch's left sidewall experienced an obvious inward deformation under the stress waves. Zhu et al. (2018) investigated the response of a tunnel under stress waves caused by different types of high explosive explosions inside its adjacent tunnel via the Universal Distinct Element Code (UDEC). The results showed that as compared to CYCLOTOL, HMX, and PETN explosions, a TNT explosion caused less response of the tunnel. Mitelman and Elmo (2014) investigated the influence of tunnel's separation distances on the response of a tunnel under TNT explosion-induced stress waves originating from its adjacent tunnel via a hybrid finite-discrete numerical approach. It was found that with the increasing separation distance, the relatively-high-velocity block ejections with small particle sizes from the tunnel wall gradually turn into low-velocity spalling failure with large blocks.

In addition, required separation distances for neighbouring tunnels have been proposed to minimize the potential threats of HE explosions occurring inside the tunnel to adjacent tunnels. Required separation distances for neighbouring tunnel-like chambers in different rock conditions have been specified in the manuals of AASTP-1 (NATO, 2010) and the US DoD 6055.09-M (DOD, 1999) based on loading densities and explosive weights. For instance, the US DoD 6055.09-M (DOD, 1999) specified that the separation distance of neighbouring ammunition storage chambers in strong rock mass should be not less than the cubic root of detonated explosive weight when the loading density is not greater than 50 kg/m^3. The fact that required separation distances in the aforementioned manuals are given only for the neighbouring tunnel-like chambers without lining support. Zhou and Jenssen (2009) proposed an equation of the required separation distance for neighbouring tunnels with lining support. The required separation distances of neighbouring tunnels mentioned above are given with specific structural configurations, geological conditions, and explosion scenarios, which are applicable for twin tunnels against HE explosion-induced stress waves. It is known that the intensities, frequencies, and durations of BLEVE-induced stress waves greatly differ from those of TNT explosion-induced stress waves, as reported in the authors' previous study (Cheng et al., 2022a). In current practice of assessing the tunnel responses to accidental BLEVE, TNT equivalence method is typically used to predict the explosion load owing to the challenges in predicting the BLEVE load, which may not give accurate predictions of structural responses. Therefore, it is of great significance to examine the response of a tunnel under stress waves induced by BLEVEs occurring inside its adjacent tunnel to ensure sufficient blast resistant capacity of twin tunnels.

In this study, the dynamic response of an arched tunnel under BLEVE-induced stress waves originating from its adjacent tunnel is numerically investigated. The numerical models of twin tunnels are established using the explicit finite element code LS-DYNA. The tunnel response under BLEVE-induced stress waves is investigated by using directly predicted BLEVE loads instead of TNT-equivalence explosion loads, which are widely adopted in existing studies and practice. Computational Fluid Dynamics (CFD) tool FLACS is used to simulate BLEVE loads acting on the inner surface of left branch of the twin tunnels. The BLEVE loads and the model of the tunnel lining and rock mass under blasting loads have been calibrated by the authors in earlier studies (Cheng et al., 2022a; Cheng et al., 2022c) and thus are not repeated herein. The response of the right branch subjected to stress waves caused by the BLEVE occurring inside the left branch are compared with that of the TNT equivalence explosion. In addition, the effects of the cover depths of tunnel, the separation distances of twin-tunnel, the concrete grades of tunnel lining, and the types of rock mass around tunnel on the response of right branch of twin tunnels under BLEVE-induced stress waves are examined.

2. Numerical model of twin tunnels

Numerical models of twin tunnels with different separation distances, cover depths, and surrounded by different types of rock masses are built in this section. The details of numerical models, including tunnel configurations, model domains, mesh details, boundary conditions, and BLEVE scenario, are presented below.

2.1. Finite element model and BLEVE loads

Fig. 1 shows the finite element model details of twin tunnels and the BLEVE scenario inside the left branch of twin tunnels. Geometric and lining configurations of the twin tunnels (see Fig. 1**(b)**) are determined according to the Qidaoliang tunnel in China (Lai et al., 2016). The tunnel lining is comprised of the lining arcs and the lining invert. The lining arcs, including the upper and lower arcs, consist of the first lining with a thickness of 0.1 m and the second lining with a thickness of 0.5 m. The inner radius of the half-circle upper arc is 5.4 m. Two lower arcs poured at both ends of the upper arc have a same inner radius of 7.9 m. The lining invert is composed of the second lining with a maximum thickness of 1.5 m and the first lining with a uniform thickness of 0.1 m. 20 mm diameter steel bars are employed as hoop, longitudinal and shear reinforcements of the second lining. 0.2 m is specified as the spacing of steel reinforcements, as shown in Fig. 1**(c)**.

The worst BLEVE scenario (i.e., the explosive flashing of 80% pressurized liquid in a tanker with the violent vapour expansion (Bubbico and Marchini, 2008; Van den Berg et al., 2006)) with the burst of a 20 m^3 Liquified Petroleum Gas tanker is considered to occur in the left branch of the twin tunnels. The BLEVE centre is located on the centreline of the left branch along *y*-direction. The distance between the tunnel floor and BLEVE centre is 1.7 m, as shown in Fig. 1**(c)**. Computational Fluid Dynamic (CFD) software FLACS is used to simulate the BLEVE scenario. The calibration of BLEVE loads by using the FLACS has been conducted by the authors (Li et al., 2022) and is not detailed herein. The BLEVE loads are then applied to the inner surface of the left branch of the twin tunnels in LS-DYNA. By balancing the computational cost and accuracy, the simulated BLEVE loads are applied to the first 8 m sections of the left branch along the tunnel length (i.e., along the *x*-direction). The first 8 m sections are divided into 8 segments with an interval of 1 m. Five parts, i.e., A, B, C, D, and E are assigned for each segment along the half cross-section, and it is assumed that the BLEVE load is uniformly distributed in each part. This simplification leads to reasonable predictions because all locations on the upper arc (i.e., A) have an equal distance from the BLEVE centre. Whereas different locations on the lower arc (i.e., B) have only slightly varying distances from the BLEVE centre. In addition, the tunnel floor is divided into three loading parts (i.e., C, D, and E) according to the variation characteristics of BLEVE loads. Through multiple numerical trials, it was found that applying non-uniform loads to each part of the tunnel floor does not result in noticeable differences in the tunnel response when compared to applying uniform loads to each part. Thus, for simplicity, uniform loads are applied to each divided part

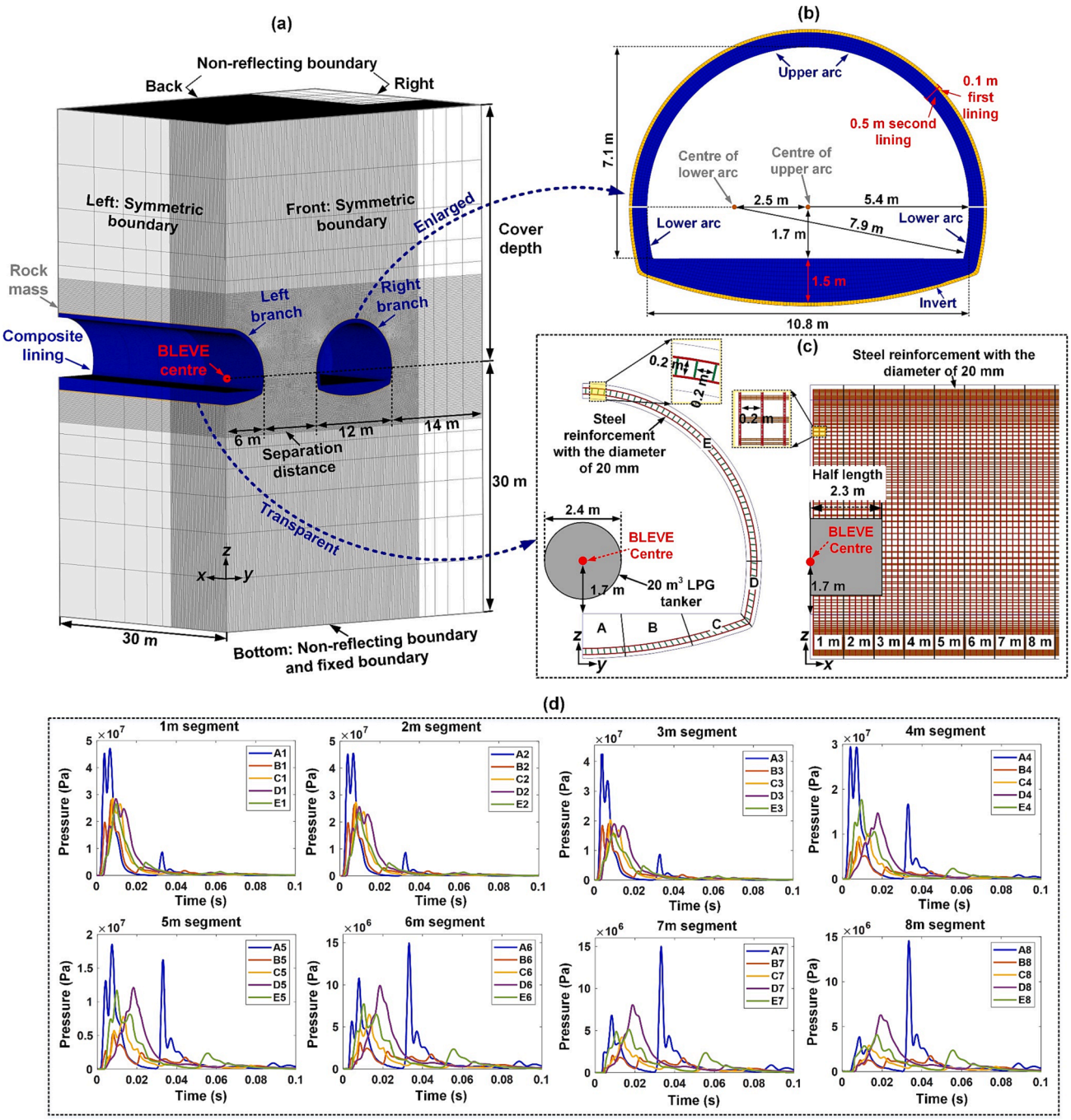

Fig. 1. Finite element model of twin tunnels and BLEVE scenario inside tunnel, (a) finite element model, (b) geometric configurations of tunnel and details of lining, (c) BLEVE loading divisions and reinforcement configurations, (d) BLEVE loads at different division segments (Cheng et al., 2022a).

along the half cross-section.

The numerical model of the twin tunnels is symmetric along its left and front surfaces. Therefore, symmetric boundaries are assigned to the model's left and front surfaces, as shown in Fig. 1**(a)**. The left branch's half cross-section is built due to the symmetry of the BLEVE loadings inside the left branch along *x*-direction. The right branch is modelled at the distance of 14 m from the right boundary of the numerical model. Furthermore, the BLEVE centre is located at 30 m from the bottom boundary of the numerical model, and the length of the numerical model along the *x*-direction is set as 30 m. The non-reflecting boundaries are assigned to the model's right, back and bottom surfaces to minimize the possible reflections of stress waves at the boundaries. Different separation distances between twin tunnels (i.e., the closest distance of sidewalls of two branches) and different cover depths of twin tunnels are considered in the study. 100 mm solid elements are employed to mesh the lining concrete and rock mass around the twin tunnels near the BLEVE centre. With the increased distance from the concerned area of twin tunnels, the mesh sizes of the lining concrete and rock mass gradually increase to save computational cost. Through mesh convergence tests, 50 mm beam elements are employed to mesh the steel reinforcing bars. The keyword *CONSTRAINED_ BEAM_ IN_ SOLID is utilized to simulate the interaction between the steel reinforcements and the lining concrete.

Table 1
Parameters of lining material model.

Lining component	Material model in LS-DYNA	Parameter	Value
Concrete	*MAT_CONCRETE_DAMAGE_REL3	Density	2300 kg/m^3
		Poisson's ratio	0.2
		Compressive strength	25, 35, 45 and 55 MPa
Steel rebar	*MAT_PIECEWISE_LINEAR_PLASTICITY	Density	7850 kg/m^3
		Young's modulus	210 GPa
		Poisson's ratio	0.3
		Yield stress	300 MPa

2.2. Material models and model calibration of road tunnel

The lining concrete, steel reinforcement, and rock mass are included in the finite element model of the twin tunnels. The models of lining concrete and steel reinforcement are given in Table 1. Density, Poisson's ratio, and unconfined compressive strength of the lining concrete are input and the remaining material parameters are automatically generated. Different grades of lining concrete for the numerical models of the twin tunnels are simulated by specifying unconfined compressive strengths. The piecewise elastic-plastic model with an ideal elastic-plastic stress-strain relationship is used for the steel rebars. Strain rate effects of steel rebars and concrete are considered by employing dynamic increase factors (DIFs) for the yield strength of steel rebars (Malvar, 1998) and the tensile and compressive strengths of concrete (Hao and Hao, 2014). The required material parameters for steel reinforcement and concrete are listed in Table 1.

According to site conditions of the Qidaoliang tunnel (Yang, 2006), three categories of rock mass, i.e., phyllite, mudstone, and sandstone are considered in this study. The numerical models of the twin tunnels surrounded by different rock mass types are built in this study. *MAT_RHT is utilized to simulate the behaviour of rock mass under blast loading. The field tests of the Qidaoliang tunnel carried out by Yang (2006) are employed to obtain the basic parameters of *MAT_RHT for three categories of rock mass. Other parameters are integrated from existing studies (Liu et al., 2018; Xie et al., 2017). The required parameters of *MAT_RHT for three categories of rock mass are listed Table 2 and Table 3.

The numerical models of the tunnel, including the rock mass and lining structures, have been calibrated in earlier studies by the authors (Cheng et al., 2022a; Cheng et al., 2022c; Li et al., 2022) based on the test of internal TNT explosions inside an underground rock chamber and the test of a RC slab subjected to a TNT explosion, respectively. To avoid repetition, only the brief calibration results are shown in Fig. 2. The details can refer to Cheng et al. (2022a) and Cheng et al. (2022c).

3. Results and discussions

In this section, the response of the right branch due to the BLEVE occurring inside the left branch is first compared to that induced by TNT equivalence explosion. The BLEVE-induced response of the right branch with different cover depths, separated by different distances from the left branch, and surrounded by different types of rock are then investigated in Section 3.2, Section 3.3, and Section 3.4, respectively.

Table 2
RHT model parameters with different values for three categories of rock mass (Liu et al., 2018; Xie et al., 2017; Yang, 2006).

Type of parameter	**Specific parameter**	**Rock type**		
		Sandstone	Mudstone	Phyllite
Basic parameters	Compressive strength (MPa)	41.0	15.3	8.4
	Elastic shear modulus (GPa)	28.0	8.2	8.8
	Density (kg/m^3)	2600	2650	2650
Strain rate parameters	Compressive strain rate dependence exponent β_c	0.028	0.061	0.088
	Tensile strain rate dependence exponent β_t	0.033	0.057	0.070
Strength parameters	Failure surface parameter A	2.70	2.86	2.91
	Failure surface parameter N	0.65	0.62	0.615
EOS parameters	Crush pressure P_{el} (MPa)	27.33	10.25	5.60
	Hugoniot polynomial coefficient A_1 (GPa)	25.36	18.32	18.18
	Hugoniot polynomial coefficient A_2 (GPa)	37.34	26.92	26.71
	Hugoniot polynomial coefficient A_3 (GPa)	21.00	11.71	11.62

Table 3
RHT model parameters sharing same values for three types of rock mass (Liu et al., 2018; Xie et al., 2017; Yang, 2006).

Type of parameter	**Specific parameter**	**Value**	**Specific parameter**	**Value**
Basic parameters	Relative shear strength	0.8	Relative tensile strength	0.08
Strain rate parameters	Reference compressive strain rate E_{0c} (s^{-1})	$3e^{-5}$	Reference tensile strain rate E_{0t} (s^{-1})	$3e^{-6}$
	Break compressive strain rate E_c (s^{-1})	$3e^{25}$	Break tensile strain rate E_t (s^{-1})	$3e^{25}$
Strength parameters	Lode angle dependence factor Q_0	0.68	Lode angle dependence factor B	0.05
	Compressive yield surface parameter G_c	0.53	Tensile yield surface parameter G_t	0.7
	Volumetric plastic strain fraction in tension P_{tf}	0.001	Erosion plastic strain E_{psf}	2
	Shear modulus reduction factor X_i	0.5	Minimum damaged residual strain E_{pm}	0.015
	Residual surface parameter A_f	0.25	Residual surface parameter N_f	0.62
Damage parameters	Damage parameter D_1	0.04	Damage parameter D_2	1
EOS parameters	Initial porosity α_0	1.0	Porosity exponent N_p	3
	Gruneisen gamma γ	0	Compaction pressure P_{co} (MPa)	6000
	Parameter for polynomial EOS B_0	1.22	Parameter for polynomial EOS B_1	1.22
	Parameter for polynomial EOS T_1 (GPa)	36.22	Parameter for polynomial EOS T_2 (GPa)	0

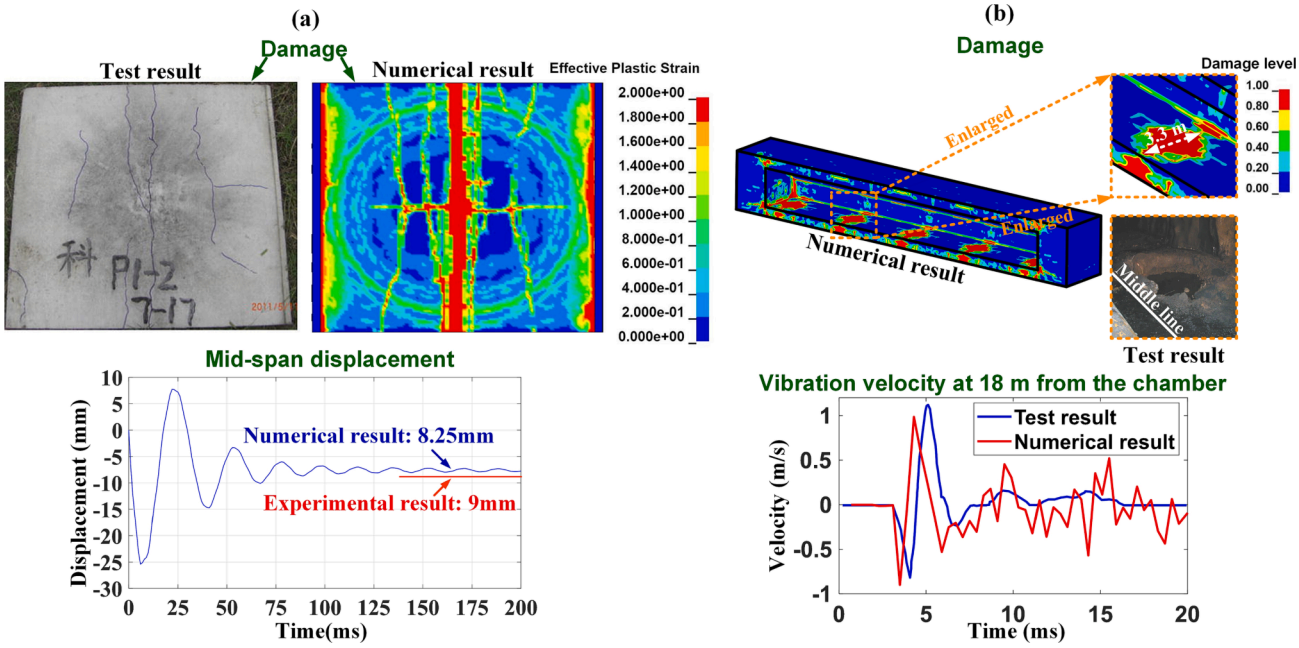

Fig. 2. The calibration results of (a) lining (Cheng et al., 2022a) and (b) rock mass (Cheng et al., 2022c).

3.1. Response difference under BLEVE and TNT explosion

To compare the tunnel responses due to stress waves caused by the BLEVE and its TNT equivalence explosion, the numerical model of twin tunnels in mudstone with the concrete strength of 25 MPa and the cover depth of 30 m is considered herein. According to JTG330.1-2018 (MTPRC, 2018), the separation distance between branches of the twin-tunnel is 6 m for the cover depth of 30 m as shown in Fig. 3, which is used herein as an extreme scenario. The numerical model of twin tunnels under BLEVE loading has been described in Section 2.1. The numerical model of twin tunnels with the case of TNT equivalence explosion is given herein, as shown in Fig. 3. An TNT equivalence explosion is assumed at the same explosion centre as the BLEVE in the left branch of the twin tunnels. 1150 kg is determined as the TNT equivalence weight of the BLEVE according to a typical TNT equivalence method of the BLEVE proposed by Prugh (1991). The TNT explosion loadings acting on the inner surface of the left branch are generated by a computational fluid dynamics (CFD) algorithm, i.e., the embedded ALE algorithm of explosive in LS-DYNA. A quarter dimension of the TNT charge and the air domain between the TNT charge and the left tunnel lining are established with the symmetric settings of the numerical model along *y*

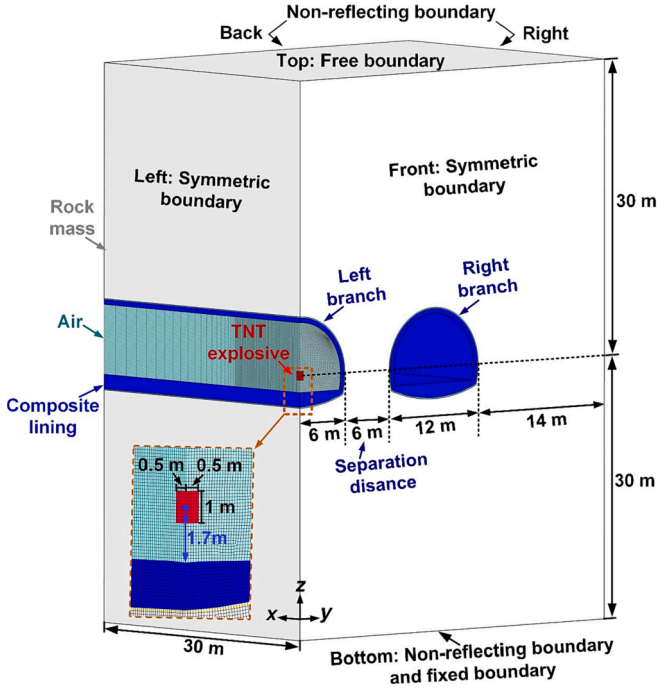

Fig. 3. Numerical model of twin tunnels subjected to TNT explosion. Note: Cover depth of arched tunnel is the distance from the centre of tunnel to ground surface.

Table 4
Parameters (Wei et al., 2009) and properties of explosive and ideal air.

Component	Material model and EOS	Parameter	Value
TNT explosive	*MAT_HIGH_EXPLOSIVE_BURN	Detonation velocity (m/s)	6930
		Chapman-Jouget pressure (GPa)	21
		Density (kg/m^3)	1630
	*EOS_JWL	Constant B (GPa)	3.747
	$P = A(1-\frac{\omega}{R_1 V})e^{-R_1 V} + B(1-\frac{\omega}{R_2 V})e^{-R_2 V} + \frac{\omega E}{V}$	Constant A (GPa)	373.8
		Constant R_1	4.15
		Constant R_2	0.9
		Constant ω	0.3
		Initial internal energy E_0 (J/m^3)	6×10^9
Air	*MAT_NULL	Density (kg/m^3)	1.225
	*EOS_LINEAR_POLYNOMIAL	Constants C_0, C_1, C_2, C_3, C_6	0
	$P_1 = C_0 + C_1\mu + C_2\mu^2 + C_3\mu^3 + (C_4 + C_5\mu + C_6\mu^2)E_r$	Constants C_4, C_5	0.4
		Initial internal energy E_{r0} (J/m^3)	2.5×10^5

Note: E and E_r are the internal energies of explosive and air per unit volume, respectively; E_0 and E_{r0} are the values of E and E_r at the initial time instant, respectively; μ is the compression parameter.

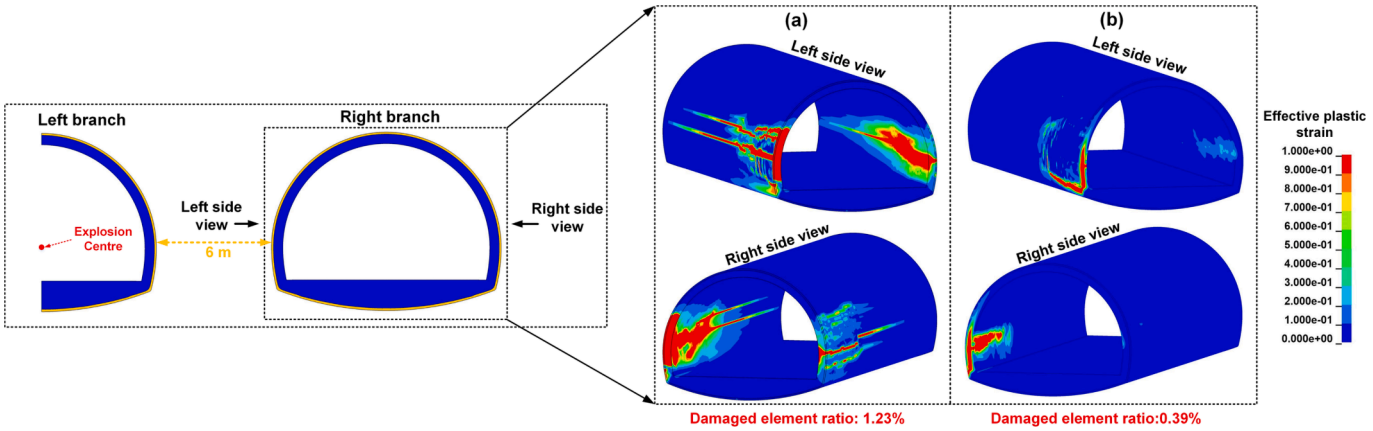

Fig. 4. Concrete damage of the right branch due to (a) BLEVE and (b) TNT explosion occurring inside the left branch.

and z directions, as shown in Fig. 3. The material models and the equations of state (EOS) of explosive and air as described in LS-DYNA keyword user's manual (LSTC, 2020) are used, as given in Table 4. 100 mm-mesh-size solid elements are used to mesh the ALE group of explosive and air domains based on mesh convergence tests. The accuracy of the ALE algorithm in simulating the explosion loads acting on the tunnel has been verified in earlier studies by the authors (Cheng et al., 2022a; Cheng et al., 2022c) and thus is not repeated herein. Other details of the numerical model can refer to Section 2.

Fig. 4 shows the concrete damage of the right branch in the cases of the BLEVE occurring inside the left branch and the TNT equivalence explosion. It is found that the concrete damage in the case of BLEVE is not only presented on the left side of the right branch, but also appears on the right side of the right branch. However, the damage of lining concrete subjected to TNT explosion is mainly developed on the left side of the right branch, and little damage occurs on the right side of the right branch. Meanwhile, the left side of the right branch in the case of TNT explosion has a less damage area than that in the case of BLEVE. The proportion of the severely damaged lining components (i.e., the red region) of the right branch subjected to BLEVE-induced stress waves reaches 1.23%, more than three times the proportion of damage caused by TNT explosion-induced stress waves. The results indicate that BLEVE-induced stress waves can cause more severe damage to the adjacent tunnel lining as compared to TNT explosion-induced stress waves.

The deformation and damage processes of lining concrete are shown in Fig. 5 to reveal the difference of lining response in the TNT explosion and BLEVE cases. At 11 ms of the BLEVE case, the tensile damage occurs on the left side of the right branch due to the reflection of stress waves at the inner surface of the lining. The lining damage on the left side of the right branch is further intensified at 16 ms with the increase of inward bending deformation of the left side wall under the BLEVE-induced compressive stress waves. At 21 ms, the inward deformation of the left side wall leads to significant upward deformation of the arched lining of the right branch and thus induces the tensile damage of the right

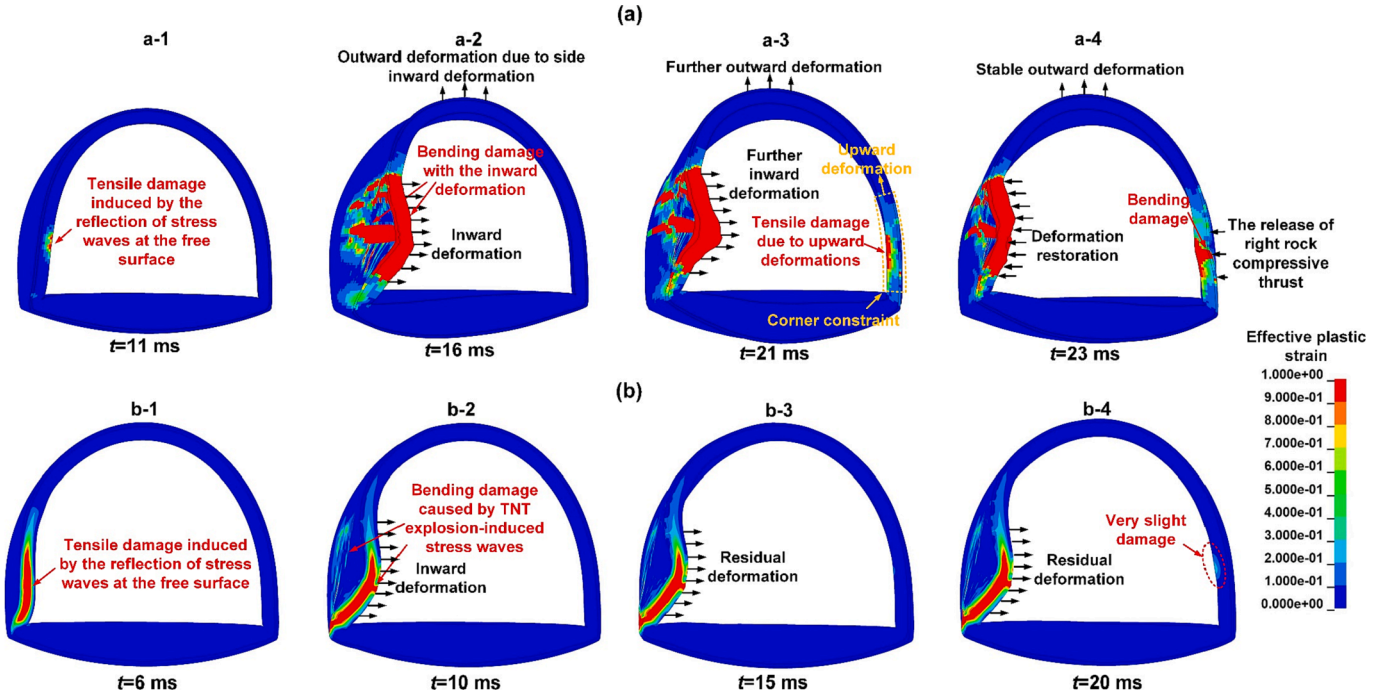

Fig. 5. Damage and deformation processes of lining concrete of the right branch under stress waves caused by (a) BLEVE and (b) TNT explosion occurring inside the left branch. Note: the deformation is magnified by 500 times for demonstration.

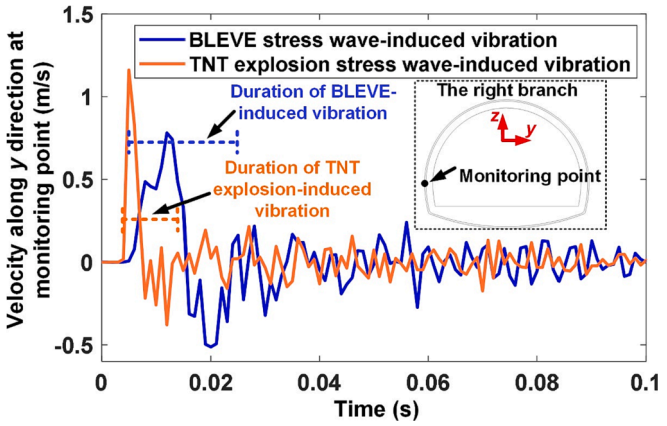

Fig. 6. Comparison of velocity response time histories along y-direction at monitoring point of the right branch induced by BLEVE and TNT explosion occurring inside the left branch.

sidewall of the right branch. At 23 ms, the inward deformation of the left side of the right branch decreases to some extents with the decreased stress wave intensity. The rebound response (i.e., the decreased inward deformation) of the left side of the right branch causes the accumulation of compressive stress between the rock mass and the right side of the right branch, which results in inward bending damage of the right side of the right branch.

Compared to the tensile damage of lining concrete due to the reflected stress waves in the case of BLEVE, the corresponding one in the case of TNT explosion is more severe, as shown in a-1 and b-1 in Fig. 5. That is because the intensity of TNT explosion-induced stress waves propagating to the left sidewall of the right branch is higher than that of the BLEVE, as indicated by the vibration intensities at the left sidewall of the right branch (see Fig. 6). However, the bending damage of the lining induced by the inward deformation of the left sidewall under TNT explosions is significantly lower than that in the case of BLEVE. The above observation is because BLEVE-induced stress waves have longer duration (see Fig. 6) and thus higher impulses, contributing to more significant deformation of the left sidewall of the right branch. In addition, TNT explosion-induced stress waves induce a more significant inertial effect of the tunnel lining than BLEVE-induced stress waves. Therefore, the compressive stress between the right sidewall of the right branch and the rock mass is much lower under TNT explosion, which only causes slight damage on the right sidewall of the right branch. Based on the

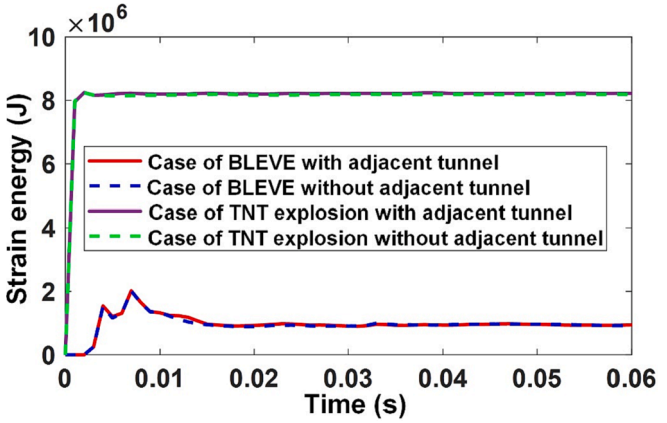

Fig. 7. Strain energy of the left branch subjected to internal BLEVE and TNT explosion in the cases with (twin tunnel) and without (single tunnel) the right branch.

above results, it is clear that the response of the tunnel under stress waves caused by the BLEVE are different from that of TNT equivalence explosion. The tunnel response under BLEVE-induced stress waves could be underestimated by using the TNT equivalence method.

To figure out whether the response of the left branch subjected to the internal explosion pressure can be significantly affected by the stress waves reflected by the right branch, two cases (i.e., twin tunnel and single tunnel) are considered. The numerical model of the twin-tunnel (i.e., the left and right branches) under the BLEVE and TNT explosion has been given above. The numerical model of a single tunnel (i.e., the tunnel without a right branch) under the same internal BLEVE and TNT explosion has been given in earlier studies by the authors (Cheng et al., 2022c). Fig. 7 shows barely no strain energy difference of lining concrete at the left branch between the two cases under either BLEVE or TNT explosion. The results indicate if the separation distance between the twin tunnels satisfies the design requirements (e.g., minimum 6 m determined based on JTG330.1-2018 (MTPRC, 2018)), the responses of the left branch subjected to internal explosion pressures are hardly affected by the existence of an adjacent tunnel. It is because compared to the stress waves directly caused by the explosions, the stress waves reflected by the right branch are relatively small when propagating to the left branch. To further investigate the adjacent tunnel's response under stress waves caused by the BLEVE, the influencing factors such as cover depth, separation distance and rock mass type are considered as follows.

3.2. *Response under different cover depths*

To examine the influence of cover depth on the response of the right tunnel branch under the BLEVE occurring in the interior of the left tunnel branch, the numerical models of the twin tunnels with four cover depths (i.e., 10 m, 30 m, 100 m, and 500 m) are built under the same type of rock mass (i.e., mudstone) and the same lining configurations (e.g., C25 concrete). It is worth mentioning that the separation distance between branches of the twin-tunnel is not less than 6 m for the case of tunnel with a 30 m cover depth, as given in Section 3.1 according to the design code JTG330.1–2018 (MTPRC, 2018). For the twin-tunnel with less cover depths (e.g., 10 m in this study), according to the design code, the separation distance between branches of the twin-tunnel needs to be increased to prevent either branch from being significantly affected by the combined stress waves reflected from the ground surface and the adjacent tunnel owing to the explosion in one tunnel, as well as those induced by the above-ground loads (e.g., vehicle-driving loads) during operation. Based on JTG330.1-2018 (MTPRC, 2018), the minimum separation distance between branches of the twin-tunnel with the cover depth of 10 m is determined as 8 m. To investigate the cover depth's effect on tunnel response, 8 m separation distance is also used in the cases of other cover depths (i.e., 30 m, 100 m, 500 m) for consistency. When the cover depth is greater than 30 m, it is found that the wave reflections from the top boundary of the numerical model, i.e., the ground surface have very limited effect on the dynamic response of the tunnel, To reduce the computational cost, only 30 m is included in the numerical models of the twin tunnels with a cover depth greater than 30 m by specifying the non-reflection boundary to the top boundaries of numerical models. However, the in-situ stresses under the four cover depths are properly calculated for each case according to the actual cover depth using the empirical relations developed by Li et al. (2016) and Brown and Hoek (1978). The calculated in-situ stresses are incorporated into the numerical models by conducting stress initialization with a quasi-static method (Yang et al., 2020). The details of the in-situ stress initialization have been given in earlier study by the authors (Cheng et al., 2022c) and thus are not detailed herein.

Fig. 8 shows the concrete damage of the right branch due to stress waves caused by the BLEVE inside the left branch in the cases of four cover depths. It can be seen that the lining damage gradually decreases as the cover depth increases from 10 m to 100 m. The reason behind it is that the lining deformation under BLEVE-induced stress waves can be

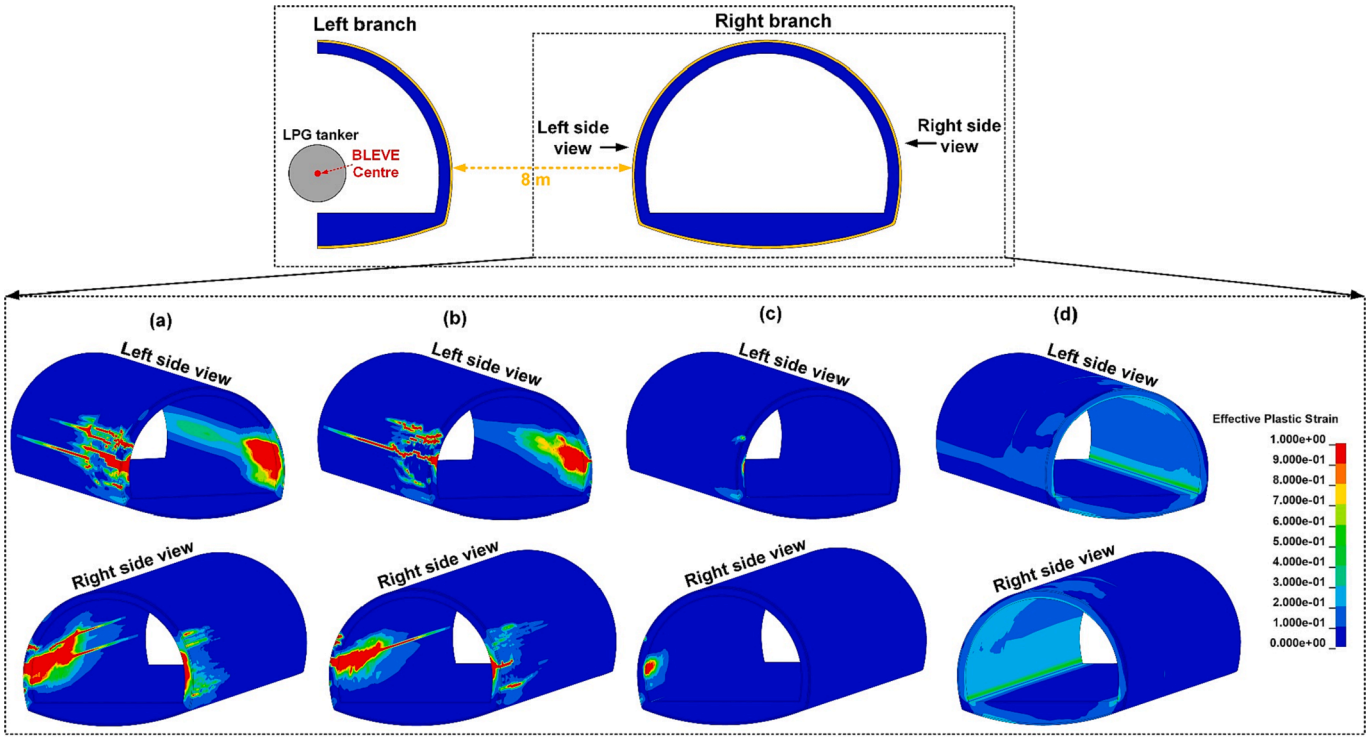

Fig. 8. Concrete damage of the right branch under the BLEVE inside the left branch in the cases with the cover depths of (a) 10 m, (b) 30 m, (c) 100 m, and (d) 500 m.

effectively constrained since the in-situ stresses of rock mass increases with the increased cover depths. However, as the cover depth increases from 100 m to 500 m, the range of lining damage increases. It is because of the large in-situ stress in the rock mass owing to the deep cover depth of 500 m, which combined with the explosion induced stresses leads more severe damages to the tunnel lining. The above results can be well explained by the strain energies of lining concrete in the cases of four cover depths, as shown in Fig. 9. The strain energy of lining concrete caused by BLEVE-induced stress waves decreases gradually from $2.036e^6$ J to $1.683e^6$ J with the cover depth increasing from 10 m to 500 m, which indicates the lining response under BLEVE-induced stress waves is gradually reduced owing to the large rock mass weight which confines the rock mass responses to the explosion load. However, the in-situ stress-induced strain energy of concrete increases gradually from $2.861e^5$ J to $9.258e^6$ J with the cover depth increasing from 10 m to 500 m. In the case with the cover depth of 500 m, an obvious higher lining strain energy is induced by the high level of in-situ stress. Among the four cover depths given in this study, the tunnel lining with the cover depth of 100 m has the lowest strain energy caused by the combined BLEVE-induced stress waves and in-situ stress. However, determining the appropriate cover depth to minimize the strain energy experienced by the tunnel lining depends on various factors, including tunnel configurations, rock properties, and BLEVE scenarios. Therefore, it is recommended to determine the most appropriate cover depth of tunnels

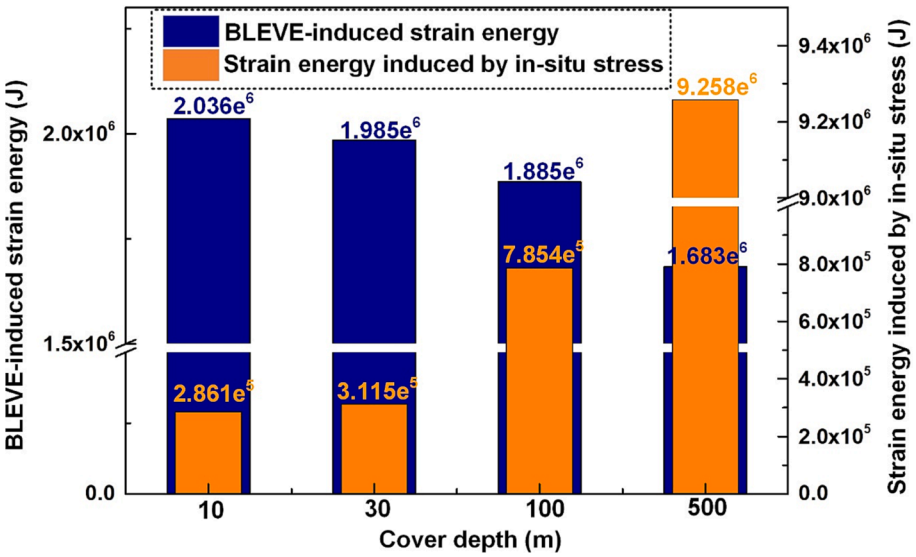

Fig. 9. Strain energies of lining concrete of the right branch induced by BLEVE-induced stress waves and in-situ stress.

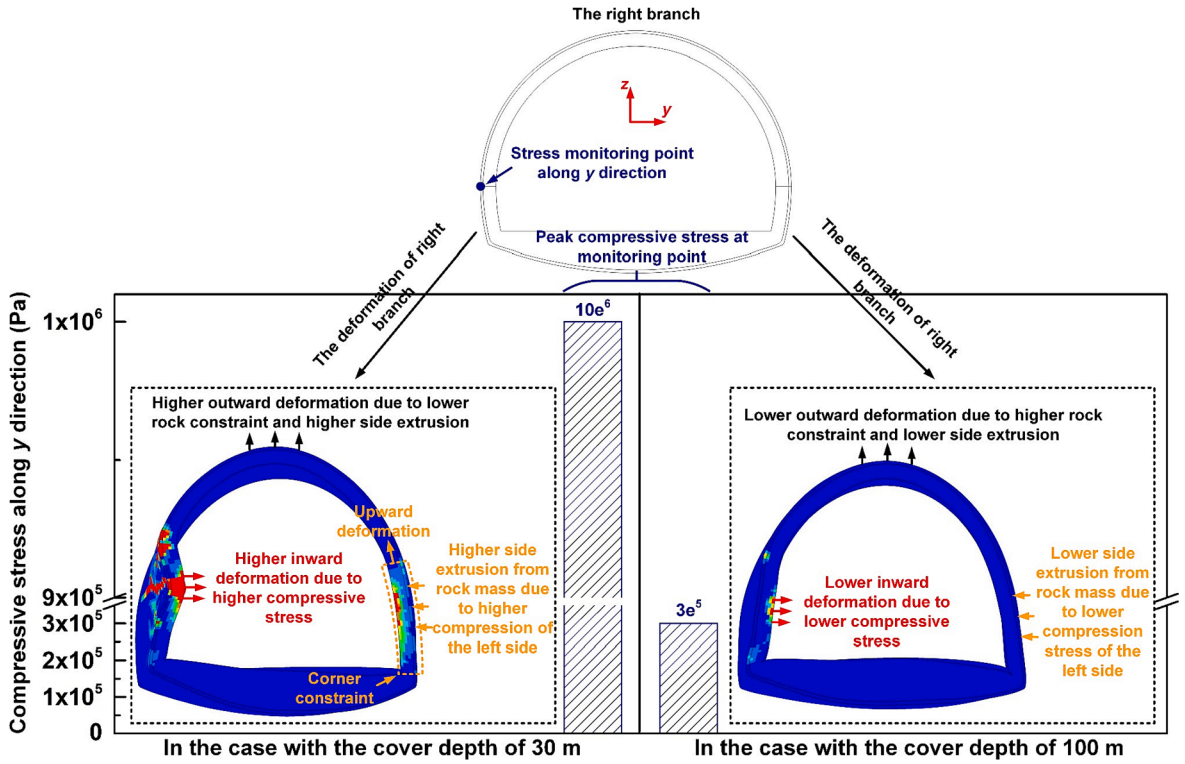

Fig. 10. Thrust of rock mass to lining at the monitoring point and deformation of lining in the case with the cover depths of 30 m and 100 m. Note: the deformation is magnified by 500 times for demonstration.

based on their specific conditions. It is worth noting that no collapse of the right branch is observed for the four cases even though the cover depth of the twin tunnel is reduced to 10 m.

As shown in Fig. 8, both sides of the right branch lining in the cases of 10 m and 30 m cover depths experience damage. However, the left sidewall of the right branch for the case of 100 m cover depth experiences less severe damage than those in the cases of 10 m and 30 m cover depth. That is because larger cover depth leads to higher in-situ stress, which can better suppress the deformation of rock mass and thus significantly attenuate the intensity of BLEVE-induced stress waves in rock mass (see Fig. 10). Meanwhile, the higher in-situ stress of rock mass with 100 m cover depth has more significant constraints on the deformation of lining concrete. Therefore, the corresponding deformation of lining concrete under BLEVE-induced stress waves is more effectively restrained, which leads to much less lining damage on the right side of the right branch in the case of 100 m cover depth. An appropriate cover-depth for the tunnel to resist BLEVE-induced stress waves can be determined by considering both the in-situ stresses and the BLEVE induced stress. It is because increasing the cover depth can decrease the tunnel response caused by BLEVE-induced stress waves whilst the intensified response of the tunnel can be induced by the increased in-situ stresses.

3.3. Response under different separation distances

To investigate the influence of separation distance between the twin tunnels on the response of the right tunnel due to BLEVE occurring inside the left branch, three numerical models of the twin-tunnel with the separation distances of 6 m, 8 m and 10 m are built in this section, respectively. Other configurations for the three numerical models such as the lining configurations, mesh details, cover depth (i.e., 100 m), rock type (i.e., mudstone), and BLEVE scenario are kept the same as those in Fig. 1.

Fig. 11 shows the concrete damage of right branch of the twin tunnels in the cases with the separation distances of 6 m, 8 m, and 10 m. It can be found that increasing the separation distances of twin tunnels can significantly reduce the response of the right branch under stress waves caused by the BLEVE occurring in the interior of the left branch. As shown, the ratio of the severely damaged lining components (i.e., the red region) of the right branch reaches 0.37% in the case of 6 m separation distance. In the cases with the separation distances of 8 m and 10 m, the ratios of the damaged lining components are 0.20% and 0.0%, respectively. The displacements on the left side of the right branch are also compared and shown in Fig. 12. 8 m is suggested as the minimum separation distance of twin tunnels in mudstone to avoid the penetrated lining damage, i.e., the damage running through the thickness of lining concrete defined by Yang et al. (2019).

3.4. Response under different types of rock mass

The above study indicates that the tunnel cover depth of 100 m and the twin-tunnel separation distance of 8 m are recommended for twin tunnels in mudstone to reduce the threats imposed by BLEVE-induced stress waves. In practice, road tunnels often run through multiple categories of rock mass along the longitudinal alignment of road tunnels. Therefore, it is necessary to investigate the effect of rock types on the tunnel response under BLEVE-induced stress waves. The numerical models of the twin tunnels with different rock masses are established in this section. Other configurations (e.g., lining configurations, mesh details and boundary conditions, as shown in Fig. 1) remain the same. Three categories of rock mass, i.e., mudstone, phyllite, and sandstone, are considered with an identical cover depth of 100 m and separation distance of 8 m.

Fig. 13 shows the concrete damage of the right branch in three categories of rock mass under the same BLEVE occurring inside the left branch. The mechanical properties of rock masses are gradually

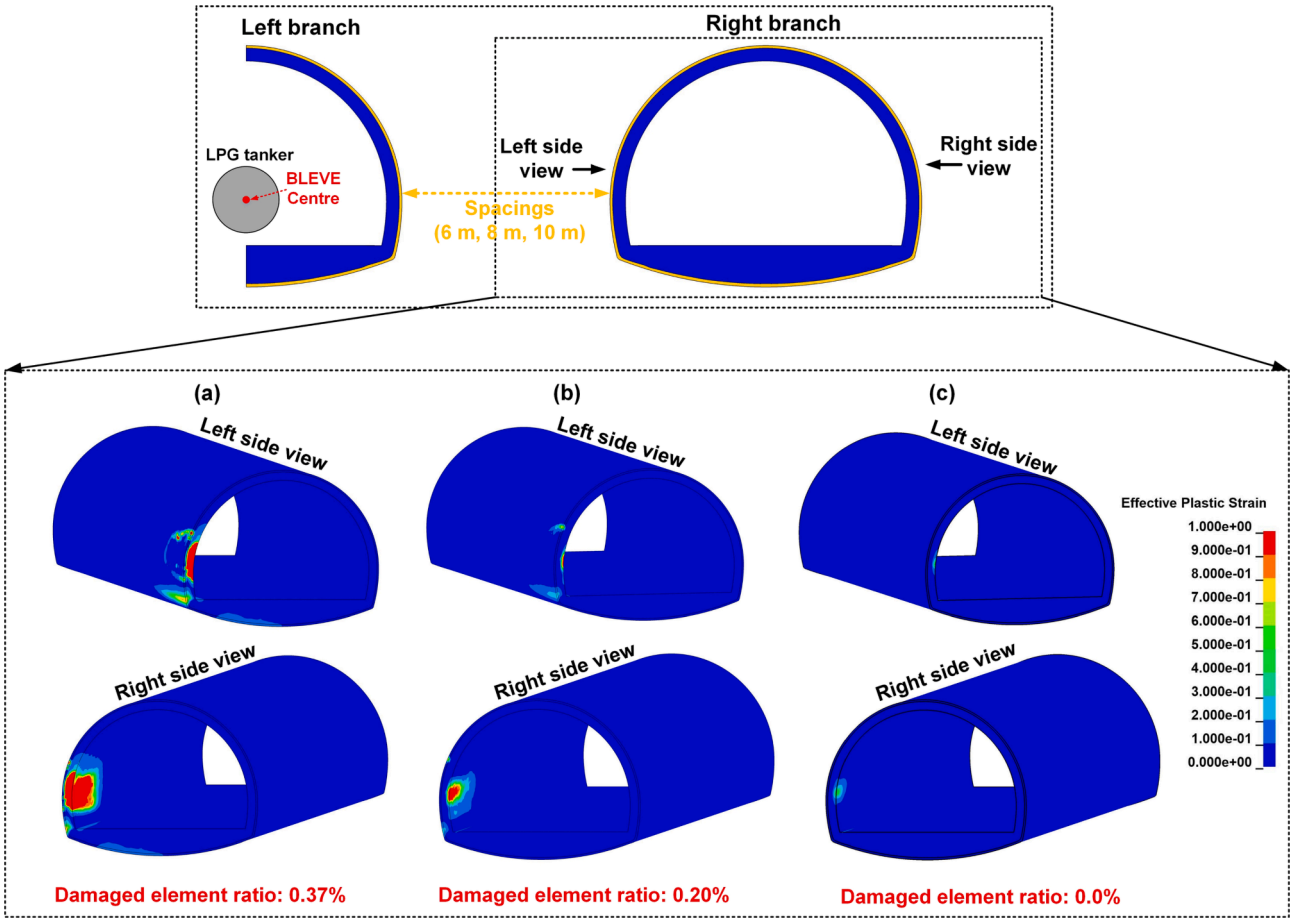

Fig. 11. Concrete damage of the right branch under the BLEVE inside the left branch in the cases with the separation distances of (a) 6 m, (b) 8 m, and (c) 10 m.

weakened from the sandstone, mudstone to phyllite. It is found that the concrete damage of the right branch decreases with the enhanced mechanical properties of rock masses. The right branch surrounded by the phyllite experiences the most severe damage among the three cases with different rock types. Quantitative results based on strain energies of lining concrete are shown in Fig. 14. The strain energies of lining concrete of the right branch are $3.3e^6$ J, $1.885e^6$ J, and $7e^5$ J for the cases of phyllite, mudstone, and sandstone, respectively. That is because rock masses with better mechanical properties can effectively constrain the lining deformation and lead to less damage to lining under BLEVE-induced stress waves. In addition, it can be seen from Fig. 13 that the damage of lining concrete of the right branch surrounded by the sandstone and mudstone does not penetrate the thickness of lining concrete. However, the corresponding damage in the case of the phyllite penetrates the thickness of lining concrete. The results indicate the separation distance of 8 m and the cover depth of 100 m are sufficient for the twin tunnels surrounded by the sandstone and mudstone to avoid severe damage (i.e., penetrated damage in this study) of the tunnel lining under stress waves caused by the BLEVE in the interior of the adjacent tunnel. However, the twin tunnels surrounded by the phyllite need be provided with the effective protective measures to mitigate the threats imposed by BLEVE-induced stress waves, which is studied in Section 4.

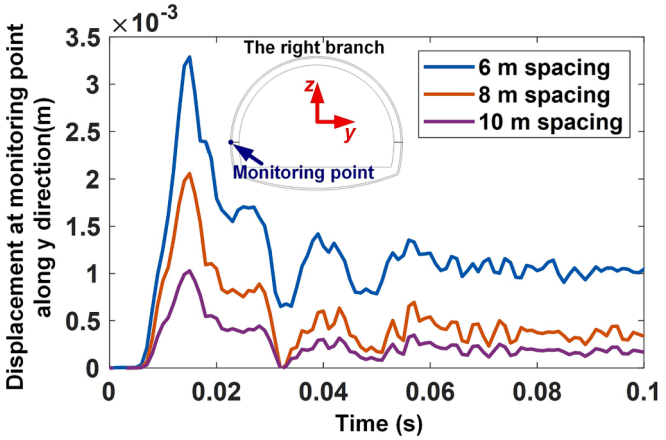

Fig. 12. Displacements along *y* direction at the monitoring point in the cases with the separation distances of 6 m, 8 m, and 10 m.

4. Case study of improving the safety of the tunnel in phyllite

As investigated in Section 3.4, given the 100 m cover depth and the 8 m separation distance, the tunnel lining surrounded by the phyllite experiences severe penetrated damage under the stress waves caused by the BLEVE occurring in the interior of the left tunnel. To improve the BLEVE resistance of the tunnel, potential measures can be employed, such as enhancing rock mass around tunnels by grouting or rock bolts, using high-performance lining concrete, improving lining configurations, and increasing separation distances of twin tunnels, etc. In engineering practice, it is easy and cost-effective to improve the performance of twin tunnels by utilizing strong lining (e.g., using high-grade of concrete) and increasing separation distances of twin tunnels. Therefore, increasing lining concrete grades and separation distances of twin tunnels are considered as feasible options for enhancing the performance of

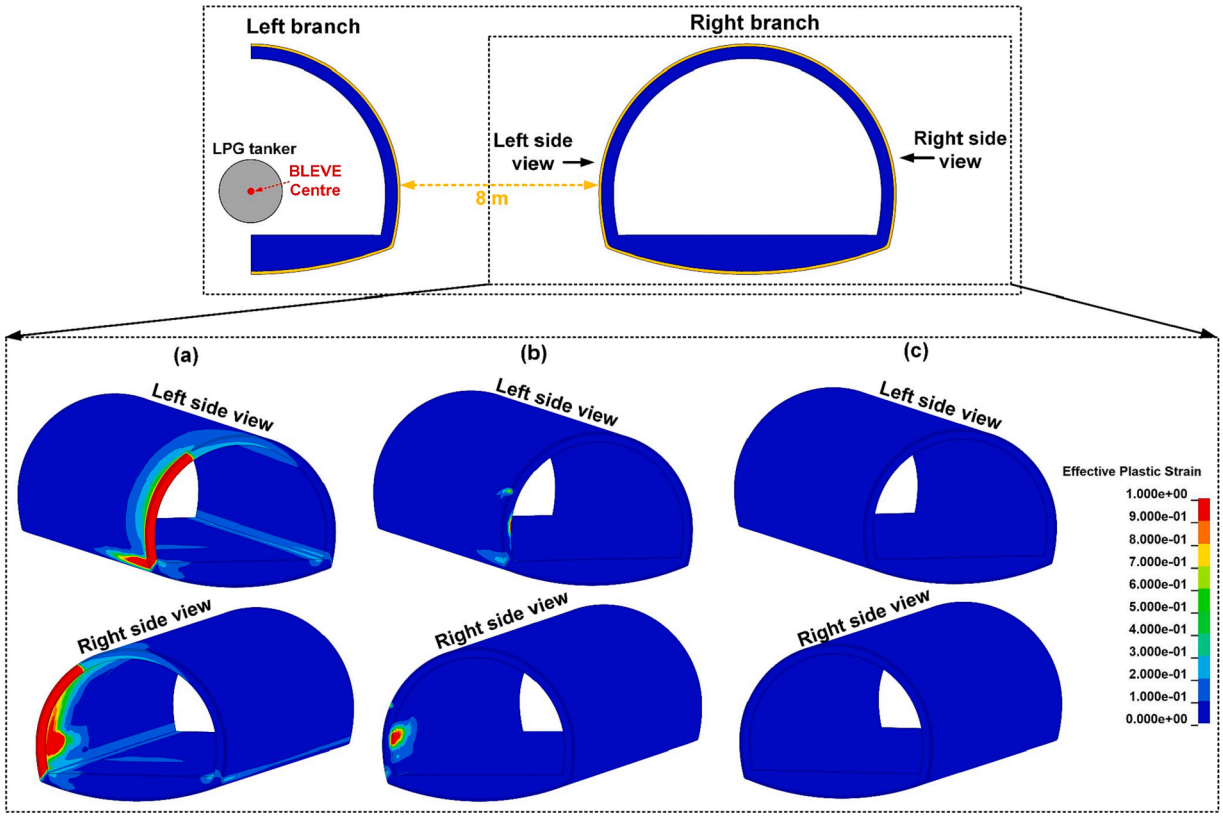

Fig. 13. Concrete damage of the right branch under the BLEVE inside the left branch in the cases of (a) phyllite, (b) mudstone, and (c) sandstone.

tunnels and safety of adjacent tunnel. The corresponding performances of using the two approaches are investigated as follows.

4.1. Enhancing concrete grades

Three grades of concrete, i.e., concrete with compressive strengths of 55 MPa (C55 concrete), 40 MPa (C40 concrete), and 25 MPa (C25 concrete) are considered as the lining concrete of the twin tunnels to investigate the performance of using stronger concrete to resist BLEVE-induced stress waves. With the 100 m cover depth and 8 m separation distance for twin tunnels in phyllite, the numerical models of the twin tunnels (similar to that in Fig. 1) with C25, C40, and C55 concrete are established. The other configurations such as the reinforcement configurations, mesh details, and boundary conditions are kept unchanged.

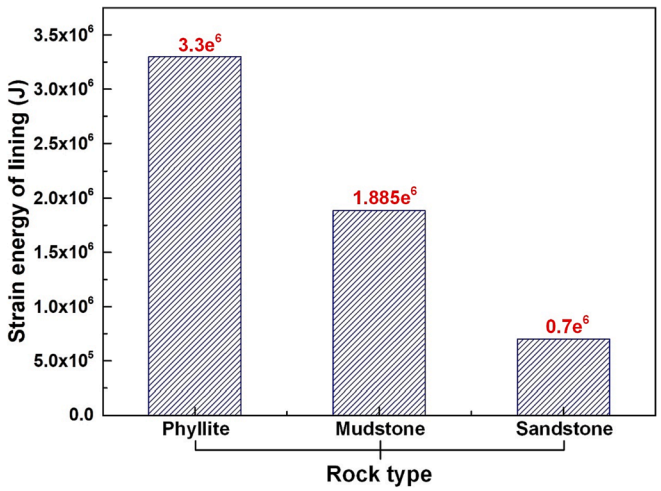

Fig. 14. Strain energy of lining concrete of the right branch surrounded by different categories of rock mass against BLEVE-induced stress waves.

Fig. 15 shows the concrete damage of the right tunnel branch against BLEVE-induced stress waves for three cases with C25, C40, and C55 concrete. It can be seen that the lining damage area of the right branch slightly decreases with the increased concrete grades. However, the penetrated lining damage of the right branch is not significantly reduced with the enhanced concrete grades. That is because the lining damage of the right branch is mainly caused by the tensile action induced by the reflection of BLEVE-induced stress waves on the inner surface of the right branch and the tensile action induced by the inward lining deflections of the right branch. The enhancement of tensile strength of concrete is limited when changing from C25 concrete to C55 concrete and it cannot effectively resist the combined tensile actions under BLEVE-induced stress waves. Quantitative results based on the strain energy of lining (see Fig. 16) also show that using stronger concrete only slightly reduces the strain energies of lining concrete. In addition, it should be noted that although the damage around the corner of tunnel lining along the cross-section with the case of the C55 concrete (see right side view in Fig. 15) is slightly lower than that in another two cases, the damage area around the corner of tunnel lining along the longitudinal direction (see left side view in Fig. 15) increases with the increased concrete grades. It may be because the wave impedance of the concrete with a higher grade can better match the wave impedance of the surrounding rock mass of the tunnel. Therefore, more BLEVE-induced stress waves in rock mass can transmit into the lining concrete of the right branch with the higher concrete grade, which increases the response of the lining corner under BLEVE-induced stress waves. Therefore, it can be concluded that using higher strength concrete is less effective in mitigating the threats of BLEVE-induced stress waves to the lining concrete.

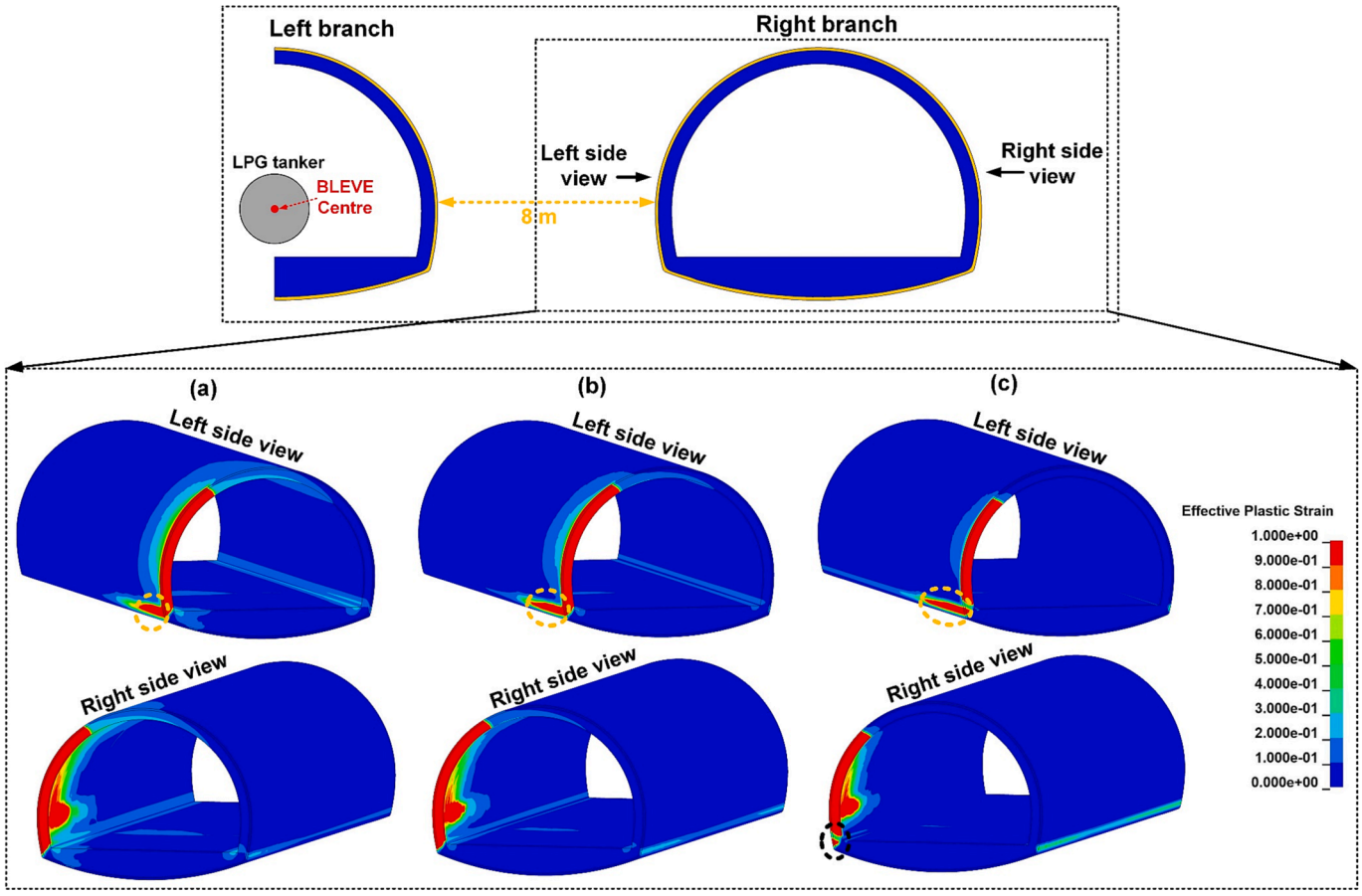

Fig. 15. Concrete damage of the right branch under the BLEVE inside the left branch in the cases of (a) C25 concrete, (b) C40 concrete, and (c) C55 concrete.

4.2. Required separation distance of twin tunnels in phyllite

Increasing the separation distance of twin tunnels can effectively mitigate the damage of lining concrete against BLEVE-induced stress waves, as discussed in Section 3.3. However, the separation distance of 8 m for the twin tunnels in phyllite is insufficient to avoid significant damage, as discussed in Section 3.4. Therefore, to determine the required separation distance of the twin tunnels in the phyllite to avoid lining damage, the numerical models of the twin tunnels with the separation distances of 8 m, 9 m, and 12 m are respectively established in this section. The other parameters for the three numerical models are kept the same as those in Fig. 1.

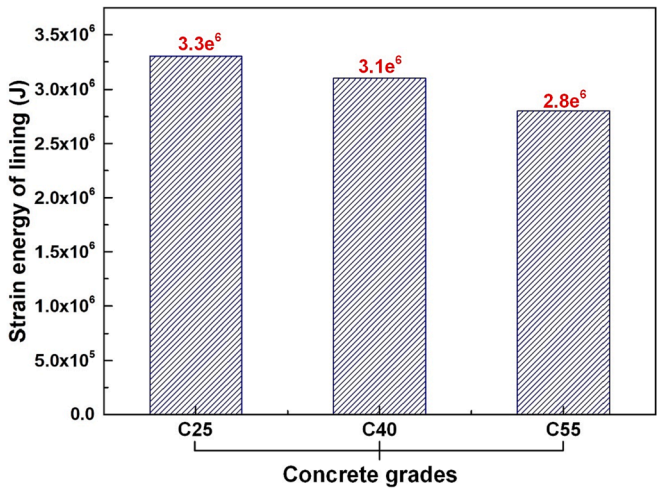

Fig. 16. Strain energy of lining concrete of the right branch with different concrete grades against BLEVE-induced stress waves.

Fig. 17 shows the damage of lining concrete of the right branch in the cases of three twin-tunnel separation distances. It is found that the concrete damage in the cases of 8 m and 9 m separation distances is severe. The damage penetrates the thickness of lining concrete in these two cases. However, when the separation distance of the twin tunnels reaches 12 m, the damage of lining concrete is less severe, and no penetrated damage is presented on the lining concrete of the right branch. The concrete's strain energy in the case of 12 m separation distance is $1.9e^6$ J, which is the lowest among the three cases, as shown in Fig. 18. Based on the above results, 12 m is required as the separation distance of the twin tunnels in the phyllite to avoid severe damage of lining under the BLEVE-induced stress waves.

5. Empirical formulae for adjacent tunnel against BLEVE-induced stress waves

The tunnel cover depth, the twin-tunnel separation distance, and the rock type surrounding the twin tunnels have significant influences on the lining response of the adjacent tunnel under stress waves caused by the BLEVE, as investigated in Section 3. Therefore, an empirical formula related to these three factors is developed to predict the intensity of BLEVE-induced stress waves acting on the adjacent tunnel. Peak particle velocity (PPV) is usually utilized as the indicator of stress wave intensity in practice. Therefore, an empirical formula with respect to PPV is proposed based on the best fit of the simulated results presented in this study, as given below.

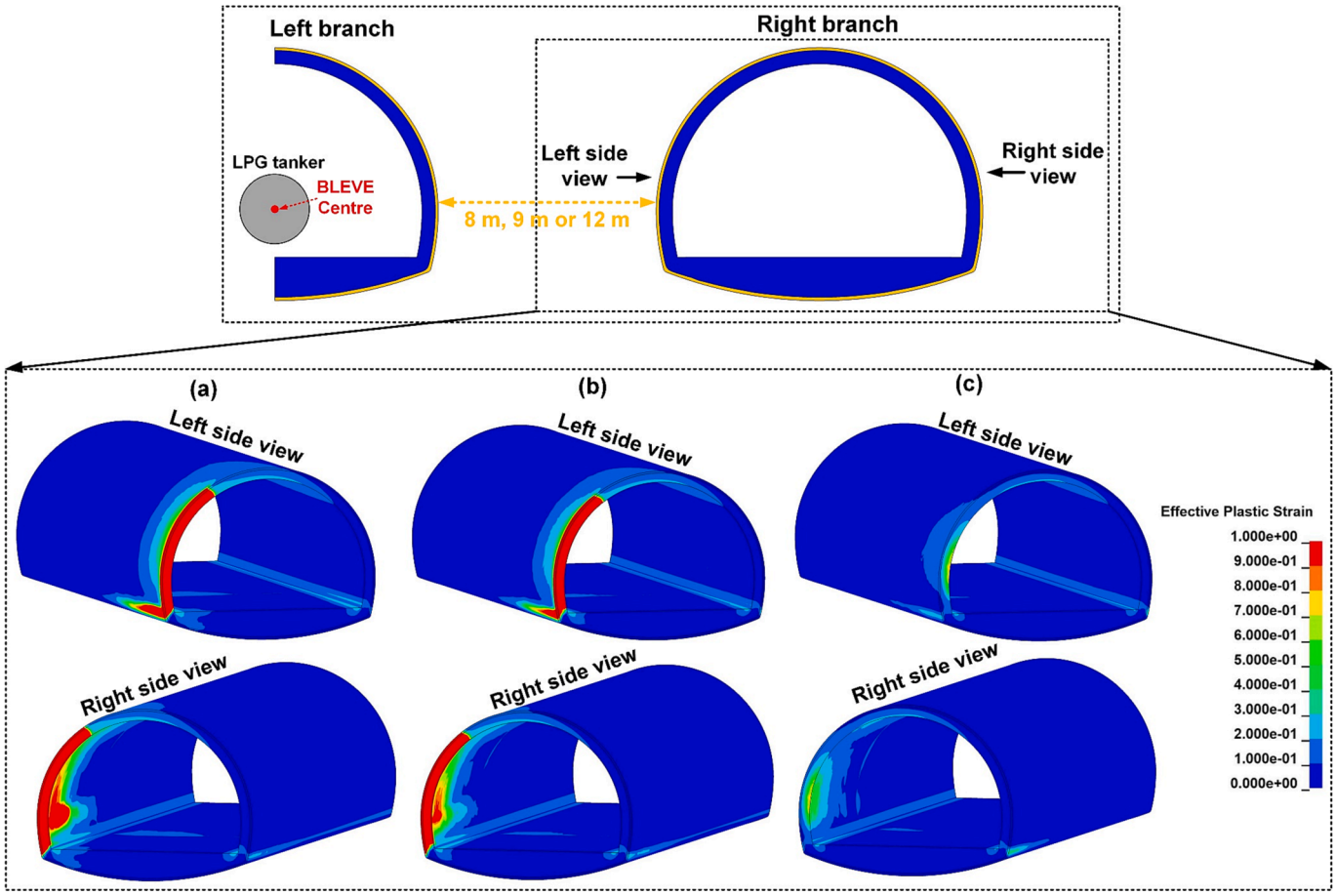

Fig. 17. Concrete damage of the right branch under the BLEVE inside the left branch in the cases with the separation distances of (a) 8 m, (b) 9 m, and (c) 12 m.

$$PPV = 16702 \times \left(\frac{R+d+l}{\sqrt[3]{Q}}\right)^{-2.196} \times (\gamma h)^{-0.366} \times \left(\frac{\rho c}{E}\right)^{0.523} \quad (1)$$

where R is the twin-tunnel separation distance (m); d is the distance (m) of BLEVE centre to the lining of the left branch; l is the lining thickness (m); Q is the TNT equivalence weight (kg) of the BLEVE assumed in this study; h is the cover depth (m) of the twin tunnels; r, ρ, c, and E are the weight density (N/m^3), density (kg/m^3), wave velocity (m/s), and elastic modulus (Pa) of the rock mass surrounding the twin tunnels, respectively.

Fig. 19 shows the comparison of the predicted and simulated peak particle velocities (PPVs) at the surface of the adjacent tunnel subjected to BLEVE-induced stress waves. The coefficient of correlation (R^2) between the simulated data and predicted results based on Eq. (1) as well as the mean value of the predicted-to-modelled ratio (M) are given. The predicted PPVs match well with the simulated data by yielding $R^2 = 0.953$ and $M = 0.997$. Therefore, given the allowable BLEVE-induced PPV, Eq. (1) can be used for the design of the twin tunnels (e.g., suggesting the safe separation distance of the twin tunnels) against the

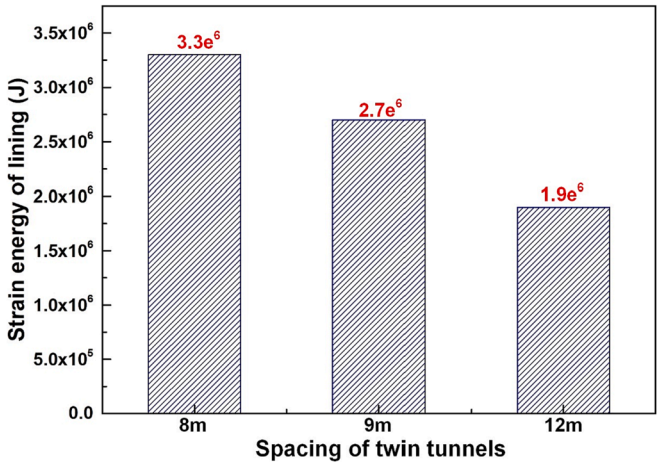

Fig. 18. Strain energy of lining concrete of the right branch of the twin tunnels with different separation distances against BLEVE-induced stress waves.

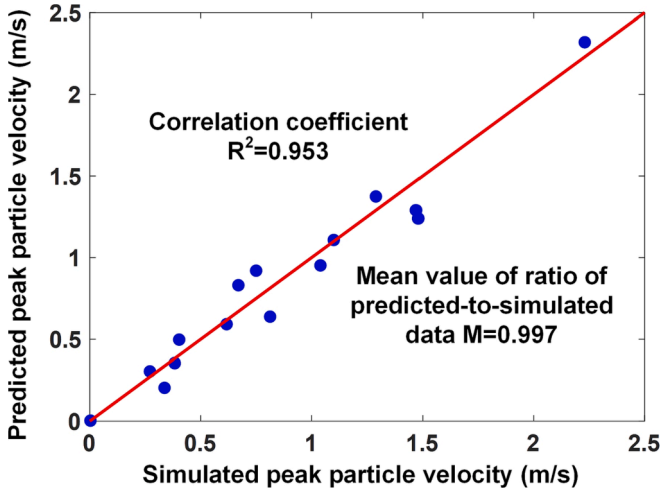

Fig. 19. Comparison of predicted values based on Eq. (1) and simulated data.

potential BLEVE occurring inside the tunnel.

To obtain the allowable BLEVE-induced PPV, an empirical formula between the dynamic tensile stress σ_t and PPV is also established according to the best fit of the simulated results presented in this study, as given by Eq. (2).

$$\sigma_t = \begin{cases} -0.20 + 6.66 \times PPV \text{ (Elastic stage, i.e., PPV}\leqslant 0.67 \text{ m/s in this study)} \\ 4.26 + 0.11 \times PPV \text{ (Damage stage, i.e., PPV} > 0.67 \text{ m/s in this study)} \end{cases} \quad (2)$$

Fig. 20 shows the simulated data and the corresponding curve-fitting results, i.e., the piecewise linear fit determined by the Eq. (2). An obvious turning point of the best-fitted curve, i.e., the dynamic tensile yield limit is observed. The allowable PPV can be determined by the dynamic tensile yield limit. The twin tunnels against BELVE-induced stress waves can then be designed based on Eq. (1). In addition, the relationship between the dynamic tensile stress and PPV under the high explosive (HE) explosion given by Dowding (1985) is compared with the empirical formula given in Eq. (2), as shown in Fig. 20. Within the elastic stage, BLEVE-induced PPV can induce higher tensile stress to the adjacent tunnel than that induced by HE explosion. With the increased PPV, the differences of tensile stresses at the same PPV between two cases gradually increase. The results indicate that BLEVE-induced stress waves with the same intensity as HE explosion-induced stress waves can impose more significant threats to the adjacent tunnel, which is attributed to the longer durations and higher impulses of BLEVE-induced stress waves.

6. Conclusion

This study investigates the response of an arched road tunnel subjected to stress waves induced by a BLEVE occurring inside an adjacent tunnel. CFD software FLACS is used to simulate the most unfavourable scenario of the BLEVE, and its loads are applied onto the inner surface of the adjacent tunnel. The response of the arched tunnel under stress waves caused by the BLEVE and its TNT equivalence explosion is compared in this study. The difference in tunnel responses under stress waves induced by the two types of explosions is identified. demonstrating the inaccuracies and possible errors of the current common practice of using TNT equivalence method in predictions of BLEVE loading effects on tunnel structures. In addition, the effects of various factors on the tunnel response under BLEVE-induced stress waves are investigated. This study provides recommendations to enhance the resistance of twin tunnels against internal BLEVE, offering valuable insights for the BLEVE-resistant design of twin tunnels. It is noted that the findings of this study are only applicable to specific tunnel configurations, BLEVE scenarios, and surrounding rock properties that were considered in the study. Therefore, it is recommended to utilize these research outcomes within the defined ranges to enhance the BLEVE resistance of twin tunnels. The main conclusions are summarized as follows.

(1) The adjacent lining damage under BLEVE-induced stress waves is more severe than that under stress waves caused by the TNT equivalence explosion due to the more severe bending damage under BLEVE-induced stress waves. Therefore, using the TNT equivalence method might underestimate the lining response of the adjacent tunnel subjected to BLEVE-induced stress waves.
(2) The stress waves due to the BLEVE inside the tunnel do not cause the collapse of the adjacent tunnel but it is very prone to induce penetrated lining damage of the adjacent tunnel with the shallow cover depth (e.g., 10 m cover depth in this study).
(3) Using stronger concrete lining cannot effectively mitigate the threats of BLEVE-induced stress waves to the adjacent tunnel. However, the adjacent tunnel response under BLEVE-induced stress waves can be effectively reduced by increasing the separation distance.
(4) To prevent the lining of adjacent tunnel from severe damage under stress waves induced by the BLEVE considered in this study, 12 m and 8 m can be respectively suggested as the minimum separation distances of the twin tunnels in the phyllite and another two-type of rock mass, i.e., mudstone and sandstone.
(5) Empirical formulae of PPV and tensile stress as a function of rock mass properties and the twin-tunnel configurations are proposed for the design of adjacent tunnel against BLEVE-induced stress waves.

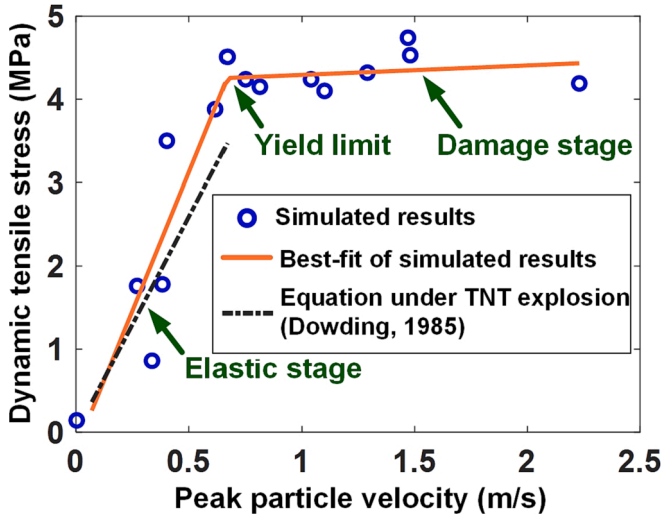

Fig. 20. Comparison of the proposed and existing (Dowding, 1985) empirical formulae.

CRediT authorship contribution statement

Ruishan Cheng: Conceptualization, Methodology, Investigation, Data curation, Formal analysis, Visualization, Writing – original draft. **Wensu Chen:** Conceptualization, Supervision, Validation, Project administration, Writing – review & editing. **Hong Hao:** Conceptualization, Supervision, Validation, Writing – review & editing. **Jingde Li:** Writing – review & editing.

Declaration of Competing Interest

The authors declare that they have no known competing financial interests or personal relationships that could have appeared to influence the work reported in this paper.

Data availability

Data will be made available on request.

Acknowledgements

The authors acknowledge the financial support from the Australian Research Council (ARC) via Australian Laureate Fellowship (FL180100196).

References

Abbasi, T., Abbasi, S.A., 2007. The boiling liquid expanding vapour explosion (BLEVE): mechanism, consequence assessment, management. J. Hazard. Mater. 141, 489–519.
Birk, A.M., 1995. Scale effects with fire exposure of pressure-liquefied gas tanks. J. Loss Prev. Process Ind. 8, 275–290.
Birk, A.M., Eyssette, R., Heymes, F., 2019. Early moments of BLEVE: From vessel opening to liquid flashing release. Process Saf. Environ. Prot. 132, 35–46.
Brown, E.T., Hoek, E., 1978. Trends in relationships between measured in-situ stresses and depth. Int. J. Rock Mech. Min. Sci. Geomech. Abstr. 15, 211–215.
Bubbico, R., Marchini, M., 2008. Assessment of an explosive LPG release accident: a case study. J. Hazard. Mater. 155, 558–565.
Cheng, R.S., Chen, W.S., Hao, H., Li, J.D., 2021. A state-of-the-art review of road tunnel subjected to blast loads. Tunn. Undergr. Space Technol. 112.
Cheng, R., Chen, W., Hao, H., Li, J., 2022a. Dynamic response of road tunnel subjected to internal Boiling Liquid Expansion Vapour Explosion (BLEVE). Tunn. Undergr. Space Technol. 123, 104363.
Cheng, R., Chen, W., Hao, H., Li, J., 2022b. Effect of internal explosion on tunnel secondary and adjacent structures: A review. Tunn. Undergr. Space Technol. 126, 104536.
Cheng, R., Chen, W., Li, J., Hao, H., 2022c. Effects of cover depth and rock type on dynamic response of road tunnels against internal explosions. Int. J. Appl. Mech. https://doi.org/10.1142/S1758825122500673.
DOD, 1999. DOD Ammunition and Explosives Safety Standards, DOD 6055.9-STD.
Dowding, C.H., 1985. Blast Vibration monitoring and control. Prentice-Hall, Englewoods Cliffs, NJ.
Feldgun, V.R., Karinski, Y.S., Yankelevsky, D.Z., 2014. The effect of an explosion in a tunnel on a neighboring buried structure. Tunn. Undergr. Space Technol. 44, 42–55.
Hao, Y.F., Hao, H., 2014. Influence of the concrete DIF model on the numerical predictions of RC wall responses to blast loadings. Eng. Struct. 73, 24–38.
Hemmatian, B., Planas, E., Casal, J., 2015. Fire as a primary event of accident domino sequences: The case of BLEVE. Reliab. Eng. Syst. Saf. 139, 141–148.
Lai, H., Wang, S., Xie, Y., 2016. Study on the Fire Damage Characteristics of the New Qidaoliang Highway Tunnel: Field Investigation with Computational Fluid Dynamics (CFD) Back Analysis. Int. J. Environ. Res. Public Health 13.
Li, X., Cao, W., Tao, M., Zhou, Z., Chen, Z., 2016. Influence of unloading disturbance on adjacent tunnels. Int J Rock Mech Min 84, 10–24.
Li, J.D., Hao, H., 2020. Numerical study of medium to large scale BLEVE for blast wave prediction. J. Loss Prev. Process Ind. 65.
Li, J., Hao, H., Chen, W., Cheng, R., 2022. Calculation of BLEVE energy and overpressures inside a tunnel using analytical and CFD methods. Tunn. Undergr. Space Technol. 120, 104263.
Li, J.C., Li, H.B., Ma, G.W., Zhou, Y.X., 2013. Assessment of underground tunnel stability to adjacent tunnel explosion. Tunn. Undergr. Space Technol. 35, 227–234.
Liu, K., Li, Q.Y., Wu, C.Q., Li, X.B., Li, J., 2018. A study of cut blasting for one-step raise excavation based on numerical simulation and field blast tests. Int. J. Rock Mech. Min. Sci. 109, 91–104.
LSTC, 2020. LS-DYNA keyword user's manual, R12.
Malvar, L.J., 1998. Review of static and dynamic properties of steel reinforcing bars. ACI Mater. J. 95, 609–614.
Mitelman, A., Elmo, D., 2014. Modelling of blast-induced damage in tunnels using a hybrid finite-discrete numerical approach. J. Rock Mech. Geotech. Eng. 6, 565–573.
MTPRC, 2018. Specifications for design of highway tunnels section 1. Civil engineering, JTG 3370.1-2018.
NATO, 2010. Manual of NATO safety principles for the storage of military ammunition and explosives AASTP-1.
Pitblado, R., 2007. Potential for BLEVE associated with marine LNG vessel fires. J Hazard Mater 140, 527–534.
Prugh, R.W., 1991. Quantitative Evaluation of "Bleve" Hazards. J. Fire. Prot. Eng. 3, 9–24.
van den Berg, A.C., van der Voort, M.M., Weerheijm, J., Versloot, N.H.A., 2004. Expansion-controlled evaporation: a safe approach to BLEVE blast. J. Loss Prev. Process Ind. 17, 397–405.
Van den Berg, A.C., Van der Voort, M.M., Weerheijm, J., Versloot, N.H.A., 2006. BLEVE blast by expansion-controlled evaporation. Process Saf. Prog. 25, 44–51.
Wei, X.Y., Zhao, Z.Y., Gu, J., 2009. Numerical simulations of rock mass damage induced by underground explosion. Int. J. Rock Mech. Min. Sci. 46, 1206–1213.
Xie, L.X., Lu, W.B., Zhang, Q.B., Jiang, Q.H., Chen, M., Zhao, J., 2017. Analysis of damage mechanisms and optimization of cut blasting design under high in-situ stresses. Tunn. Undergr. Space Technol. 66, 19–33.
Yang, H.J., 2006. Deformation characteristic of tunnel surrounding rock under complex conditions. J Railw Eng Soc 1, 57–60.
Yang, J., Liu, K., Li, X., Liu, Z., 2020. Stress initialization methods for dynamic numerical simulation of rock mass with high in-situ stress. J. Cent. South Univ. 27, 3149–3162.
Yang, G.D., Wang, G.H., Lu, W.B., Yan, P., Chen, M., 2019. Damage assessment and mitigation measures of underwater tunnel subjected to blast loads. Tunn Undergr Space Technol, p. 94.
Zhou, Y.X., 2011. Earthquakes as a rock dynamic problem and their effects on rock engineering structures. Advances in Rock Dynamics and Applications. Taylor and Francis Group, London, pp. 457–481.
Zhou, Y.X., Jenssen, A., 2009. Internal separation distances for underground explosives storage in hard rock. Tunn. Undergr. Space Technol. 24, 119–125.
Zhu, J., Li, Y., Wu, S., Zhang, R., Ren, L., 2018. Decoupled explosion in an underground opening and dynamic responses of surrounding rock masses and structures and induced ground motions: A FEM-DEM numerical study. Tunn. Undergr. Space Technol. 82, 442–454.